Unraveling Reversible Quenching Processes of O_2, N_2, Ar, and H_2O in Metal Halide Perovskites at Moderate Photon Flux Densities

Edgar R. Nandayapa, Katrin Hirselandt, Christine Boeffel, Eva L. Unger, and Emil J. W. List-Kratochvil*

Metal halide perovskites (MHP), as used in photovoltaic (PV) applications, show a rich photophysics in inert and ambient atmosphere. The presence of atmospheric molecules leads to processes that enhance as well as reduce their photoluminescence (PL) emission. Various phenomena are previously described for a wide variety of gas molecules and different classes of MHP, with a particular interest on the long-term stability for PV applications. However, reversible PL quenching (PLQ) processes, which may be regarded equally important for the performance of PV and other optoelectronic applications, are neglected in other studies. This holds true for O_2 and H_2O, but especially for low-reactive gases such as nitrogen and argon. Using low excitation densities, it is shown that noticeable—and reversible—PLQ, in addition to PL enhancements, can already be observed for O_2, N_2, and Ar as well as for H_2O at low concentrations of 1 mbar. The nature and origin of the quenching processes are further elucidated by applying the Stern–Volmer analysis, also employed to determine whether static and dynamic PLQ processes happen for the different quenching gases. The strongest static PLQ is found for O_2 and H_2O. MHPs in N_2 and Ar atmospheres display a moderate PLQ effect.

1. Introduction

In recent years, the photovoltaic (PV) community has concentrated on the development of metal halide perovskite materials (MHP), leading to a deeper understanding of the material properties and a rapid improvement of solar cell efficiencies.[1–4]

E. R. Nandayapa, K. Hirselandt, Dr. E. L. Unger, Prof. E. J. W. List-Kratochvil
Helmholtz-Zentrum für Materialien und Energie GmbH
Brook-Taylor-Straße 6, Berlin 12489, Germany
Dr. C. Boeffel
Fraunhofer Institute for Applied Polymer Research
Geiselbergstraße 69, Potsdam-Golm, Berlin 14476, Germany
Prof. E. J. W. List-Kratochvil
Department of Chemistry
Department of Physics and IRIS Adlershof
Humboldt-Universität zu Berlin
Brook-Taylor-Str. 6, Berlin 12489, Germany
E-mail: emil.list-kratochvil@hu-berlin.de

However, to push the efficiency of this material class further, it is important to understand nonradiative recombination pathways upon photoexcitation under inert conditions as well as in the presence of atmospheric gases. Photoluminescence (PL) quantum efficiency, along with time resolved photoluminescence, provides easy-to-access key parameters that assess the quality of perovskite materials. Such techniques have been adopted by a vast number of groups to study the physical properties of MHP materials of different composition.[5–7] Yet, the effect that H_2O, O_2, and other gases have on the MHP PL has mostly been investigated under high power illumination with photon flux densities surpassing 10^{20} photons s^{-1} m^{-2}, i.e., the equivalent of 100 suns and more.[5,6,8] Most of these studies focus on the degradation mechanisms of the material and the long-term stab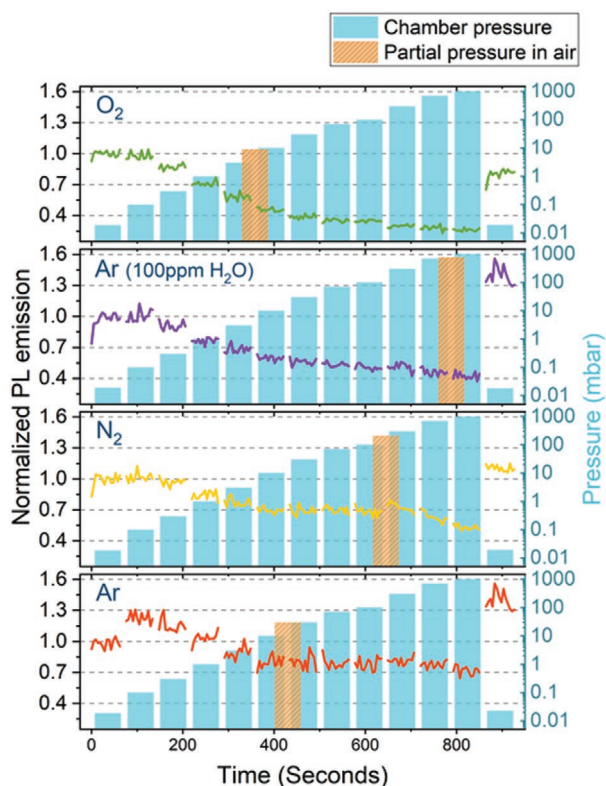ility of devices under diverse environmental conditions. However, the immediate and reversible PL quenching (PLQ) in MHP by different atmospheric molecules, at discrete pressure points and at low excitation densities of 1–10 suns, have not yet been looked at systematically. Given the fact that solar cells mostly operate at such moderate excitation density conditions, it is therefore obligatory to study the ongoing photophysical processes in more detail within this low excitation regime.

In this report, we present a systematic study on the nature of second-order PLQ effects of O_2, N_2, Ar, and H_2O on the so-called triple cation perovskite, or CsMAFA, containing cations of cesium, methylammonium (MA), and formamidinium (FA) as well as a mixture of bromide and iodide as anions. CsMAFA was chosen as a model material due to its superior film formation and stability, as opposed to the more common methylammonium lead triiodide ($MAPbI_3$).[9,10] We, however, note that all findings presented here also hold true in $MAPbI_3$ under low excitation densities.[11] By examining the PL emission and PL lifetimes, second-order quenching processes induced by the tested gas molecules, namely O_2, N_2, and Ar, as well as for H_2O, are investigated quantitatively. The Stern–Volmer (SV) analysis is then applied to PL emission and lifetime measurements at different partial pressures for each gas to identify the nature of the quenching process and the underlaying diffusion kinetics.

Figure 1. Emission intensity of perovskite under O_2, H_2O, N_2, and Ar atmospheres. Columns represent the gases pressure in mbar, with scale on the right. PL emission was measured for 2 min at pressures of 0.03, 0.1, 0.3, 1, 3, 10, 30, 70, 100, 300, 700, and 1000 mbar. All emission curves are normalized to the average value of the first measurement, in vacuo, where the sample is still pristine. For reference, partial pressures of O_2, H_2O, N_2, and Ar in atmospheric air are marked as orange columns at 210, 30, 781, and 9 mbar, respectively.[12]

2. Incremental Quencher Concentrations and PLQ

Figure 1 shows the effect that O_2, H_2O, N_2, and Ar have on the PL emission of a 600 nm CsMAFA thin film at different partial pressures. Starting from a vacuum level of 3×10^{-2} mbar, the integral PL is monitored for 2 min. This process is repeated at increasing discrete pressure values up to ambient pressure. Water-enriched argon, containing 100 ppm of H_2O, was used to study the influence of H_2O. All gases, including H_2O, displayed a substantial PLQ effect, being O_2 the strongest and Ar the weakest. The effect of O_2 is already noticeable at the low concentration of 0.3 mbar, rapidly reaching 70% of the PL of a pristine sample at a mere 1 mbar of pressure. The PL emission is further quenched to 26% when the chamber is filled to 1000 mbar of O_2. Similarly for H_2O, an equivalent PLQ trend is visible reaching a minimum of 37% of its initial PL emission at a pressure of 1000 mbar. Molecular nitrogen also shows a noticeable PLQ, decreasing by almost 15% at a pressure of 1 mbar. This reduction of PL emission continues down to 51% at a pressure of 1000 mbar. Here, N_2 displays a considerable quenching effect at small partial pressures that has previously not been reported. Finally, Ar first shows a minor increase of PL emission at pressures of 0.1 and 0.3 mbar. Afterward, there is a
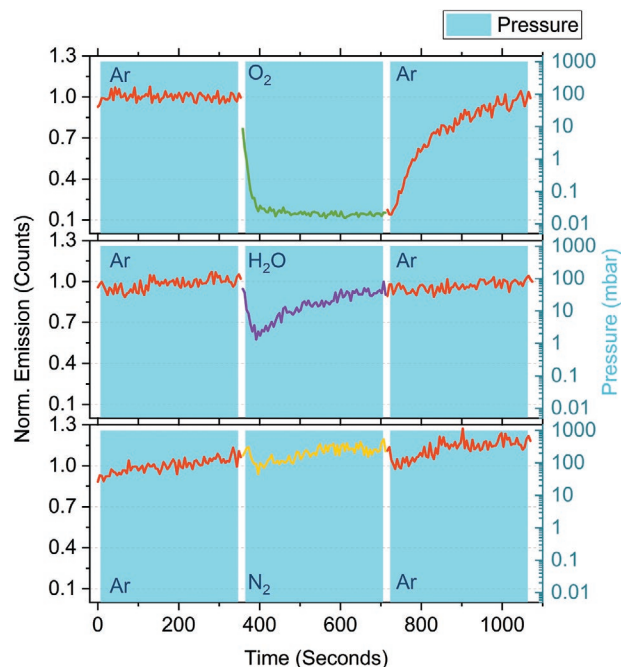
Figure 2. Resulting PL emission of samples from changing the atmosphere of the chamber from a constant flow of argon, then either to O_2, H_2O, or N_2, and finally back to Ar. Each flowing step lasted 360 s. The strong quenching effect caused by O_2 and H_2O is proportional to the one shown in Figure 1, where the sample was initially held in a vacuum.

continuous decrease of the PL emission, reaching a minimum of 66% of the initial PL intensity at a pressure of 1000 mbar. Importantly, PL intensities shown by the pristine sample are recovered and surpassed when samples are set back to vacuum conditions for all gases, with exception of O_2 were only 80% of the initial PL can be regained.

Our samples showed a clear, but reversible, PLQ effect with all gases. However, to account for possible artifacts induced by low pressure conditions, a supplementary experiment was performed. In this new experiment, the changes in PL emission by the gases were measured under a constant pressure of 1 atmosphere, as shown in **Figure 2**. Here, the samples were first placed under a constant flow of argon. 360 s later, the flow was immediately switched to either O_2, water-enriched argon or N_2 for additional 6 min, and finally back to a constant flow of argon. At first, all samples show an unchanging PL emission during the constant argon flow. Then, a rapid reduction of the PL emission is noticeable when O_2 and water-enriched argon are added into the chamber, reaching 13% and 57% of the initial PL, respectively. When the flow is switched back to a pure argon flow, the PL fully recovers over a time of 360 s for both O_2 and H_2O, indicating the reversibility of the process. Nevertheless, by closely examining the PLQ trend induced by these two gases, a clear difference is apparent. For O_2, the PL emission drops to 13% as soon as the gas is added and stays constant while O_2 flows into the chamber. In the case of H_2O, the PL emission rapidly decreases to 57%. However, the PL starts to recover almost immediately back to the level of the pristine PL while H_2O is still flowing into the chamber. This effect indicates a difference in the quenching process and dynamics of

**ADVANCED
SCIENCE NEWS**
www.advancedsciencenews.com

**ADVANCED
OPTICAL
MATERIALS**
www.advopticalmat.de

these two molecules that will be further discussed in Section 3. Finally, the effect of N_2 is almost indistinguishable from that of argon. This is because, as discussed for Figure 1, the PLQ effect of Ar and N_2 on the MHP is proportionate. This makes the change on PL emission from switching atmospheres from one to the other barely noticeable.

Previous reports have shown that existence of volatile components in the MHP crystal lattice at the surface and bulk of the crystallites could incur into significant changes of the optical properties under vacuum conditions.[13,14] Yet, this experiment demonstrates that the PLQ phenomena measured on both conditions—in vacuum and at atmospheric pressure—are analogous.

At this point it is important to note that the excitation light used on these experiments had a mean photon flux density of 10^{19} photons s^{-1} m^{-2}. The range of illumination intensities achievable by our instrument are shown in Figure S1 in the Supporting Information. Nevertheless, the excitation density used in our experiments corresponds to 10^{16} cm^{-3}, which is within the trap density found in triple cation perovskites.[15,16] The MHP samples showed an average PL quantum yield of 3.5%. Additionally, even though some of these gases have shown to alter the band bending at the perovskite surface, it has also been shown that flat band conditions can be achieved using excitation sources of either UV or visible light.[17]

Regarding the issue of stability, we found that after having added a full cycle of partial pressures of gas to the MHP layers, the change of PL emission would remain constant during consecutive cycles with the same gas. This is shown in Figure S2 in the Supporting Information, where the effects of O_2 and H_2O, the strongest PLQ molecules, were monitored during three cycles of gas addition. For instance, PL emission decreased by 20% after the first full cycle of O_2 and no evident further changes occurred during the two consecutive cycles. This behavior is opposite when using water-enriched argon. Here, the PL emission increased after the first round, keeping this increment during the following cycles. Since the change in PL emission across all pressures remains essentially the same for both gas molecules during the last two cycles, we dismiss any immediate degradation of the crystal structure due to O_2 or H_2O.[7,18,19]

Finally, the H_2O condition of these experiments refers to water-enriched argon. Water concentrations of <0.5, 10, 50, and 100 ppm in argon were considered and their effect is shown in Figure S3 in the Supporting Information. The quenching effect of the two higher concentrations showed almost no difference. Thus, to ensure the effect of H_2O, all tests were done with a concentration of 100 ppm of water in argon.

3. Analysis of PLQ Mechanisms

Earlier reports discussing the effect of environmental gases on different perovskite species, mostly $MAPbI_3$, have indicated that oxygen molecules can bind to iodide vacancies distributed throughout the perovskite lattice, mostly at the bulk.[20] The resulting trapped oxygen can later be oxidized further by excitations in the lattice, leading to the formation of superoxide. This highly reactive molecule can accelerate the degradation of the perovskite crystal.[7,19,21,22] Furthermore, the binding of oxygen to the lattice, in both $MAPbI_3$ and $MAPbBr_3$, results in an increment of the PL emission. Here, oxygen is filling up deep trap states leading to the passivation of sub-bandgap states and enhancing the emission.[5,6,23–25] This PL enhancing effect by oxygen can be further controlled by adjusting the incident photon dose illumination to the samples.[26] However, under very intense light conditions these layers undergo other types of photoinduced and degradation effects. Although without the use of concentrators or high intensity lasers, such conditions are hard to achieve.[27–29] By the same token, the formation of superoxide has been proposed as a charge-transfer mechanisms from an excited perovskite crystallite to an oxygen molecule.[18,30] In this regard, Tian and collaborators introduced the issue of dynamic and static quenching processes for oxygen in perovskite layers.[5]

Additionally, the interaction of water with perovskites has also been studied in detail, mainly focusing on how the water molecule breaks the crystal structure.[31–34] Nevertheless, it has been shown that water physisorbs to the surface of the MHP, resulting on an increase of the n-type nature of the material and a reduction of the perovskite work function.[35] The opposite happens with oxygen, where the n-type character of the surface is reduced.[35] Notwithstanding, the resulting band bending at the surface caused by these molecules, which could be as high as a few hundreds of meV, can be reverted to flat band conditions upon illumination with UV or visible light.[36] Yet, second-degree quenching effects of molecular nitrogen and argon has not been reported in the literature up until now.

Grain boundaries have been widely studied by the community, especially for their role in lowering the efficiency of solar cells and light emitting diodes.[13,37] Defects at grain boundaries have been imaged using electron backscatter diffraction, showing that amorphous regions are sites of enhanced radiative recombination.[38] Correspondingly, groups have successfully mitigated the negative effect of these grain boundaries and increased the efficiency of devices by using different cations[39–43] and molecules[44–48] as passivators.

Considering the evidence found in the literature and the experimental results shown earlier, **Figure 3** displays schematics of our proposed second-order energy transfer mechanisms for O_2, H_2O, N_2, and Ar to MHP crystallites and a discussion follows.

In our measurements, a reduction of PL emission was recorded after having added O_2 to the layers under both conditions—at low partial pressures and under a constant flow of gas at 1 atmosphere. This outcome agrees with other reports, where O_2 diffuses into the bulk of the perovskite crystallites under illumination due to light-induced phase-segregation.[22,25] However, as shown in Figure S2a in the Supporting Information, the PL emission is permanently reduced only after the first cycle of incremental gas addition and these changes remain constant during the additional cycles. After this permanent loss of emission, at least 80% of the initial vacuum PL is always recovered. This suggests that the diffusion into the bulk is limited and capped at one point.

Moreover, PLQ by oxygen molecules has been widely reported in the literature in a diverse range of nonperovskite molecules and compounds.[49,50] As shown in Figure 3a, energy transfer is possible due to the two degenerate antibonding
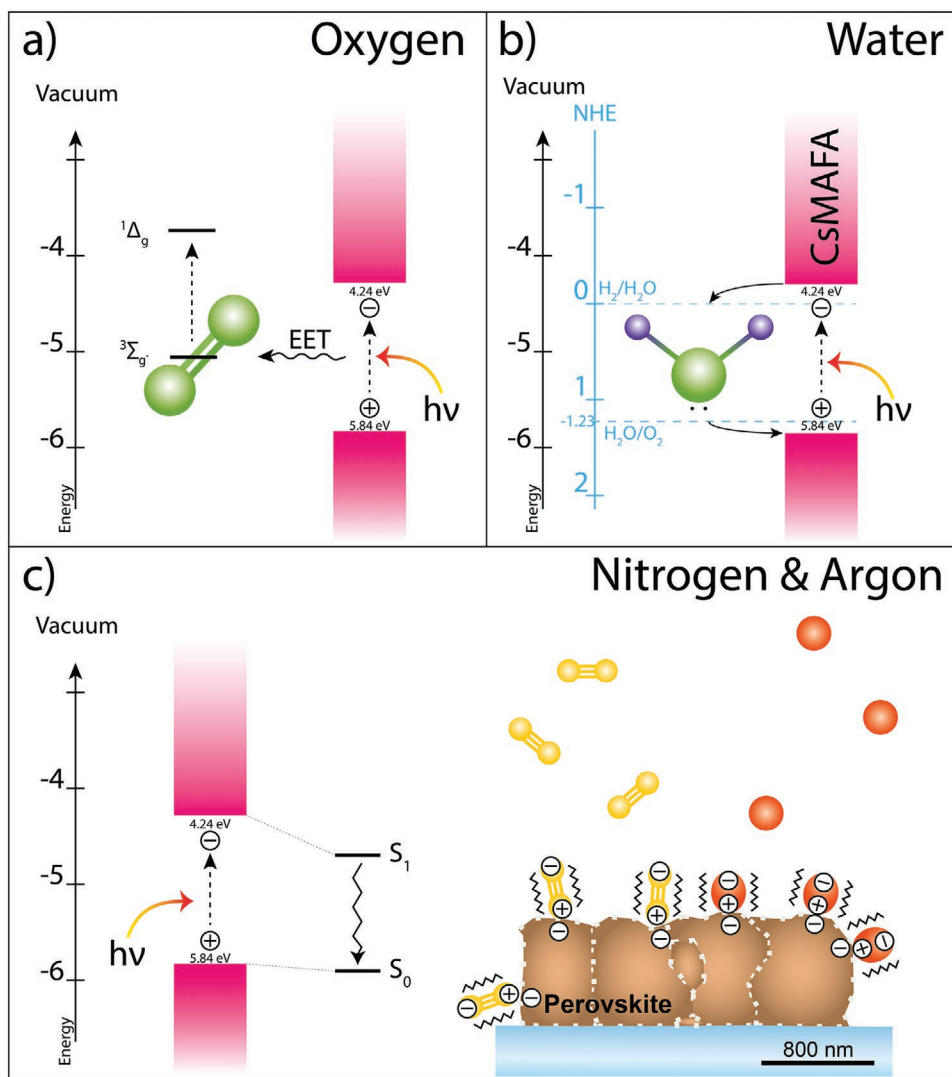
Figure 3. Quenching mechanism diagrams of O_2,[67] H_2O, N_2, and Ar on CsMAFA layers. NHE stands for normal hydrogen electrode.[61] Valence band value of perovskite from Zu et al.[36]

π-orbitals formed by the highest occupied molecular orbital of the oxygen molecule, creating an electronic ground state in the triplet state.[51] In the case of perovskites, electron–hole pairs have a low binding energy and do not show an explicit excitonic nature in most low bandgap MHP at room temperature.[52] According to simple spin statistics, freely recombining dissociated electron–hole pairs are expected to produce three correlated triplets for every singlet state upon meeting. Similar to organic materials, these states are regarded as dark states for inorganic semiconductors, releasing photons slowly.[53] This means that the excited state of the MHP emitter can be transmitted to the oxygen ground triplet state by means of a Dexter-type resonant energy transfer upon collision with the gas molecules.[54,55] As depicted in Figure 3a, this process de-excites the emitter to the ground state, quenches the PL, and excites the oxygen molecule into a singlet state, the so-called superoxide.[21] This superoxide is highly reactive and the additional charge makes it easy to bind to other molecules, in the case of the perovskites being the most preferred at the iodide vacancies.[20]

In the case of H_2O, there are reports that perovskite devices show an improvement of power conversion efficiency and other optical properties when exposed to small concentrations of H_2O during preparation.[56–58] At the same time, many other publications have focused on the degradation processes that these layers undergo when in contact with H_2O.[33,34,59,60] Our experiments show that H_2O has a strong but reversible PLQ effect on triple cation perovskites. Moreover, as it will be discussed below, there is evidence that the quenching process of H_2O is of a dynamic nature. This means that, differently from the other tested molecules, water molecules do not attach to excited perovskite crystallites, but de-excite them whenever they bounce off the crystals. Correspondingly, as shown in Figure 3b, standard reduction potentials for water-splitting closely align with the valence and conduction bands of the triple-cation perovskite.[61] This shows that it is possible for an excited perovskite crystallite to transfer both—electrons and holes—to a water molecule via a redox process. Previous results by Nickel et al. show that molecular oxygen and hydrogen are

**ADVANCED
SCIENCE NEWS**

www.advancedsciencenews.com

**ADVANCED
OPTICAL
MATERIALS**

www.advopticalmat.de

produced during the degradation of MAPbI$_3$ when exposed to oxygen via the generation of a hydroperoxyl radical and methylamine.[30] In spite of this, water splitting by MHPs is implausible since four electrons are needed to do a full redox cycle, in other words, the reduction of two water molecules into separated oxygen and hydrogen molecules.[62,63] Instead, a half reaction is likely occurring, namely $2H_2O + 2e^- \rightarrow H_2 + 2OH^-$, which has a potential of 0.83 V.[61] In this respect, hydroxide anions are known to have a strong PLQ effect resulting in a triplet state quenching and allowing a Brønsted–Lowry type proton transfer in larger molecules.[64–66] Moreover, Figure 2b presents further evidence that only a half reaction is happening. After an initial strong PLQ upon exposure to H$_2$O, the PL emission increases while under continuous illumination and a constant stream of water-enriched argon. Based on these findings, a redox process mediated PLQ, as depicted in Figure 3b, can very well account for the observations made.

The PLQ mechanisms of N$_2$ and Ar are based on Van-der-Waals (VdW) forces, as depicted in Figure 3c. In the literature, argon is known to form VdW complexes with other materials under specific conditions.[68–71] These VdW complexes can induce a distortion on the electronic orbitals of both, the gas molecule and the crystallite, enhancing the probability of converting an electronic excitation to vibrational energy.[72] Hence, an induced surface dipole is formed with adjacent argon atoms to the perovskite crystal, depopulating the excited state of the emitter via an electrostatic interaction. However, this interaction is not intense, leading to a weak PLQ effect on the emission of MHPs.

Nitrogen, also a low reactive gas, shows a distinguishable PLQ among our samples. Similar quenching effects have been found for N$_2$ in doped metal oxides, as it is the case for ZnO:Au.[73] Yet, the charge transfer mechanisms for this process have not been well reported in the literature. Nonetheless, similar to the case of argon, N$_2$ may also form VdW complexes with an excited emitter resulting in the transfer of electronic excitation to vibrational energy. The combined electron cloud of the double nitrogen forming the molecule would enhance the VdW interaction with the excited perovskite crystallites, leading to a more intense PLQ effect than argon, as it is shown in our results. Nevertheless, further experiments are needed to unmistakably identify the exact nature of the quenching mechanisms shown for Ar and N$_2$.

4. Analysis of PLQ Dynamics Based on Stern–Volmer Model

It has been widely shown in the literature that charge generation in perovskites is predominantly in the form of free charges at low excitation densities.[74,75] As a result, recombination is mostly trap-assisted, making it a first order recombination process.[76] However, bimolecular annihilation becomes more prevalent when the excitation density increases.[77] The rate equation in a perovskite film can be described by[51]

$$\frac{dn}{dt} = G - k_{tr}n - \gamma n^2 + k_q[Q] \tag{1}$$

where G is the generation rate of electrons and holes, k_{tr} is the monomolecular recombination coefficient, γ is the bimolecular

annihilation constant, k_q is the quenching coefficient, n are the concentrations of electrons, and $[Q]$ is the concentration of quenchers.

During these experiments, the excitation density used on the MHP layers was kept on the 10^{18}–10^{19} cm^{-3} range. As explained earlier, this excitation level is well within the trap density of our material. This means that the internal recombination of the crystals remained within the monomolecular recombination regime, which in turn indicates that the lifetime of the generated charges is independent of the excitation density. This information becomes relevant later for the discussion of Figure 5. Notwithstanding, PLQ involves an excited perovskite crystallite which transfers either an electron or energy to a quencher. This intermolecular process involves two separate parts: an emitter and a quencher, emphasizing that the recombination process for PLQ is always of the bimolecular type.

Second-order quenching processes like PLQ have been extensively studied with the SV analysis. This is a standard technique most commonly used in organic chemistry to study the diffusive nature and charge transfer kinetics from a fluorescent emitter to a mobile quencher.[78,79] Although this technique is generally employed to describe the quenching effect of molecules in solution,[80–84] it has also been successfully used in the soft-matter and solid state. In many of these cases, emitters are distributed and immobilized in a gas permeable thin film.[85–90] Generally, the SV analysis requires the tracking of either the PL intensity or the PL lifetime of an emitting sample that is in contact with a quencher at different concentrations. The resulting change of PL emission is then interpreted to be dynamic, static or a combination of both quenching mechanisms. Dynamic quenching, also called collisional quenching, refers to a process in which mobile quenchers de-excite crystallites in an excited state whenever they come into contact. Equivalently, static quenching refers to a process where a quencher is physisorbed to an emitter, forming a complex with it and quenching it instantly and permanently.[55]

For a standard semiconductor, radiative and nonradiative recombination always occur under steady state conditions. This can be denoted by $\gamma_{st} = k_{nr} + k_r$, where γ_{st} is the steady-state decay rate, and k_r and k_{nr} are the radiative and nonradiative recombination, respectively. Also, the excited state lifetime is the inverse of the decay rate as $\tau = \gamma_{st}^{-1}$. The concentration of fluorescent particles $[F]^*$, without the effect of any quencher, is described by

$$\frac{d[F]^*}{dt} = f(t) - \gamma_{st}\left[F^*\right]_0 = 0 \tag{2}$$

where $f(t)$ is the constant excitation function. In the presence of quenchers this process becomes

$$\frac{d[F]^*}{dt} = f(t) - (\gamma_{st} + k_q[Q])\left[F^*\right] = 0 \tag{3}$$

where k_q is the decay rate in the presence of quenchers. The SV model is the fluorescence ratio between these two different states, expressed as[91]

$$\frac{F_0}{F} = \frac{I_0}{I} = \frac{\gamma_{st} + k_q[Q]}{\gamma_{st}} = 1 + k_q\tau_0[Q] = 1 + K_{SV}[Q] \tag{4}$$

where I and I_0 are the PL emission with and without quencher, respectively, K_{SV} is the Stern–Volmer constant, k_q is the bimolecular quenching constant, τ_0 is the emission lifetime without quencher, and $[Q]$ is the concentration of the quencher. This equation models the behavior of both, static and dynamic types of quenching.[55,80] Nevertheless, for emitters that are distributed in a layer, as it is the case for perovskite crystallites (Figure S5, Supporting Information), some emitters are more accessible to the quenchers than others due to the size and stacking of the crystals on the film. A multiple site quenching model is more suitable for this situation to properly model the phenomenon. In this context, the following equation has been widely used on the quenching of polymeric films, which also display different levels of accessibility to the emitters[92–94]

$$\frac{I_0}{I} = \left[\sum_i \frac{f_{0i}}{1 + K_{SVi}[Q]} \right]^{-1} \quad (5)$$

In our case, we use a simplified version of this model, considering only two general quenching sites, the so-called two-site model. In this model, the first type of quenching site is easy to reach and is located at the surface of crystallites. The second type of quenchers are harder to access and are located at the grain boundaries. This two-site model is described by

$$\frac{I_0}{I} = \left[\frac{f_{01}}{1 + K_{SV1}[Q]} + \frac{(1 - f_{01})}{1 + K_{SV2}[Q]} \right]^{-1} \quad (6)$$

where f_{01} and $(1 - f_{01})$ are the fraction of total emitters from two components of different accessibility, K_{SV1} and K_{SV2} are the SV constants for the first and second component and $[Q]$ is the quencher concentration.

Figure 4 shows the result of fitting the average emission value at each pressure point from Figure 1 using Equation (4) (blue line) and Equation (6) (dashed golden line). To ease the visibility of details, Figure S4 in the Supporting Information displays these results with the x-axis on a logarithmic scale. The parameters resulting from fitting these data with Equations (4) and (6) are shown in **Table 1**. The Stern–Volmer constant, K_{SV}, corresponds to the slope at which the PLQ evolves. For the normal model it is only possible to fit the values up to a pressure of 10 mbar since the linear correlation reduces dramatically below 0.93 beyond this point. In general, the values yielded by the normal model are quite comparable for all gases tested. H_2O displays the largest slope with a value of 3625, closely followed by O_2, N_2, and finally Ar, which shows the smallest increment with a value almost ¼ of that by H_2O. Comparatively, the two-site model provides more detailed information since it encompasses the full range of pressures tested. Table 1 also includes a column with the weighted K_{SV} average values with respect to the fractional accessibility values that can be directly compared with the results from the normal model. In the case of $K_{SV,1}$, the values for all gases are many orders of magnitude higher than those of $K_{SV,2}$, showing that surface crystallites are much more easily reachable. Specifically, N_2 shows the largest $K_{SV,1}$, followed by H_2O, O_2, and finally Ar, while for $K_{SV,2}$, oxygen has the largest value, followed by H_2O, N_2 and finally Ar. By considering the fractional access of quenchers to
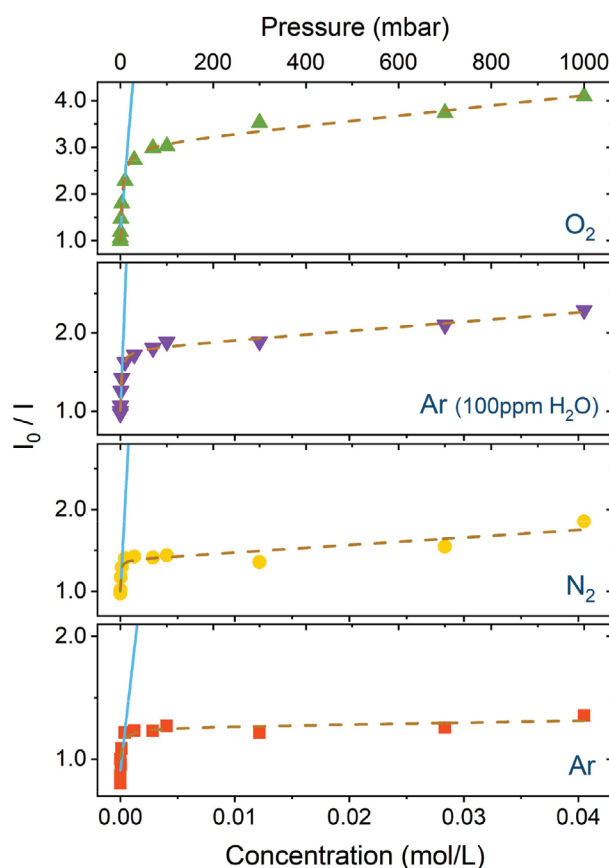

Figure 4. Stern–Volmer plot for the emission of perovskite under Ar, N_2, O_2, and water-enriched argon atmospheres. Solid curve in blue shows the fitting of normal SV model, from Equation (4). Dashed golden curve shows the fitting of the two-site SV model, from Equation (6). Fitting parameters are found in Table 1.

the emitters, f_{01} and f_{02}, we can see that 67% and 44% of crystallites are rapidly quenched by O_2 and H_2O, respectively, before reaching a pressure of 10 mbar. Correspondingly, 20% and 28% are quenched by Ar and N_2 in this pressure range. In other words, more than half of emitters accessible at the surface of the MHP are strongly quenched by O_2 and H_2O by the time a pressure of 10 mbar is reached. On the other hand, Ar and N_2 have a higher influence at higher pressure values, respectively, where grain boundaries defects become accessible. Moreover, there is evidence of saturation of quenchers, since at higher

Table 1. Fitting parameters resulting from applying the normal (Equation (4)) and the two-site (Equation (6)) SV models to the curves shown in Figure 4.

	Normal model	Two-site model				
	K_{SV}	f_{01}	$K_{SV,1}$	f_{02}	$K_{SV,2}$	$K_{SV\text{-}WA}$[a]
Ar	811.7	0.20	4728.0	0.80	1.17	946.5
N_2	2584.2	0.28	26 748.1	0.72	6.58	7494.2
O_2	2953.7	0.67	14 975.9	0.33	8.59	10 036.7
H_2O	3625.2	0.44	17 303.2	0.56	6.54	7617.1

[a]Weighted average.
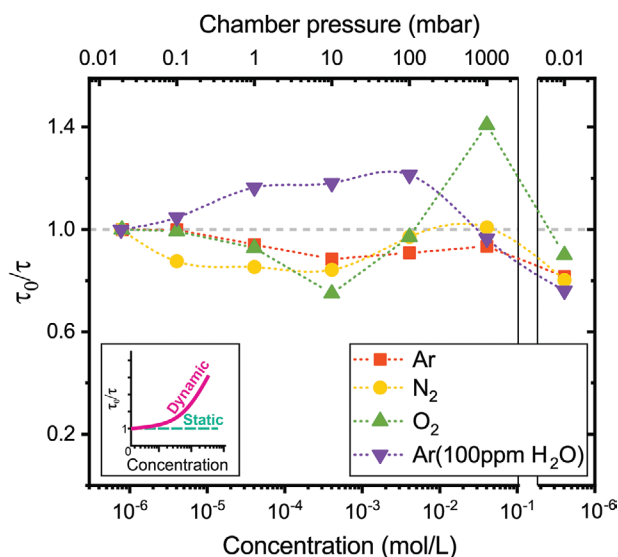
Figure 5. SV analysis applied to the PL lifetime of perovskite samples under increasing partial pressures of the quenching gases. The average PL lifetime of the pristine samples was 1656 ± 234 ns. Dotted lines are guides to the eye. Inset shows the typical behavior of dynamic and static quenching. Note that the x-axis is displayed in log-scale to match that of the main plot, so the expected linear increase of a dynamic quenching appears instead as an exponential growth.

Table 2. SV constants, K_{SV}, and bimolecular quenching constant values, k_q, resulting from fitting the normal and two-site SV models using Equations (4) and (6). For reference, 1 mol L^{-1} is equal to 1 molar [M].

	Normal model		Two-site model	
	K_{SV} [M^{-1}]	k_q [M^{-1} s^{-1}]	K_{SV} [M^{-1}]	k_q [M^{-1} s^{-1}]
Ar	811.7	4.90×10^8	946.5	5.72×10^8
N_2	2584.2	1.56×10^9	7494.2	4.53×10^9
O_2	2953.7	1.78×10^9	10 036.7	6.06×10^9
H_2O	3625.2	2.19×10^9	7617.1	4.60×10^9

existence of dynamic quenching processes that are masked by stronger static quenching and passivation effects. These results are evidence that dynamic and static quenching, in addition to passivation, are all playing a role simultaneously in the perovskite under the presence of quenchers and that their effect is reversible once they are removed.

Table 2 shows the corresponding bimolecular quenching constants for each one of the tested gases according to the normal (Equation (4)) and the two-site (Equation (6)) models. Here, the K_{SV} values for the normal and two-site model correspond to those shown in Table 1. The bimolecular quenching constant, k_q, is the result of dividing the K_{SV} constant by the lifetime of the pristine sample, as stated in Equation (4). Here, H_2O shows the largest bimolecular quenching constant for the normal model, while O_2 does for the two-site model. In all cases, the resulting value for the two-site model are slightly higher than those from the normal model because it encompasses the full range of pressures, although all values remain in the same order of magnitude. Specifically, O_2, H_2O, and N_2 show a small variation between each other. Ar, on the other hand, shows the smallest constant value by one order of magnitude lower. In general, all recombination constants are well below the diffusion-controlled limit of 10^{10} M^{-1} s^{-1}.[95] In the case of O_2, a molecule that has been widely tested in other materials, the bimolecular quenching constant value of 6.06×10^9 M^{-1} s^{-1} is comparable to the one measured in other organic molecules and dyes.[87,88] To our knowledge, the constants have not been measured for H_2O, N_2, or Ar in any other solid state materials.

The results of the SV-analysis show that the PLQ effect of O_2 and H_2O are very efficient at the surface, since more than half of PLQ occurs at a low pressure. In contrast, Ar and N_2 have a weaker interaction with the crystallite in general but becomes slightly higher at the boundary defects.

These results highlight the negative effect that low concentration of contaminant gases in gloveboxes, namely O_2 and H_2O, can have in the performance of MHP devices since they show sensitivities at partial pressures as low as 1 mbar. Nevertheless, these effects are reversible in vacuum conditions and are diminished with the use of argon, and to lesser extent with nitrogen, atmospheres.

pressures the PLQ rate slows down for all gases. The two-side model effectively describes the PLQ behavior across all pressure values, emphasizing the unbalanced accessibility of the gases into the MHP films.

By measuring the PL lifetime of the perovskite at different quencher concentrations, the SV-analysis can discriminate static from dynamic quenching processes. Similarly to Equation (4), the ratio of *unquenched lifetime* and *lifetime influenced by a quencher* should either show a linear growth behavior, in the case of dynamic quenching, or a constant lifetime ratio for static quenching.[91] The reason that static quenching results in a constant PL lifetime throughout a range of quencher concentrations is that unperturbed emitters will continue to emit as usual while complexed emitters are just permanently quenched. Conversely for dynamic quenching, the PL lifetime is affected by the collision rate of the quenchers, effectively reducing it at higher concentrations.

Figure 5 shows the change of PL lifetime of a perovskite sample with respect to the concentration of gases. Here, the lifetime change with increasing concentration for all gases is almost negligible, i.e., the lifetime ratio of unquenched and quenched crystallites is close to 1, highlighting a predominantly static quenching process. It should be stressed though, that this effect is reversible not only because the samples recover their PL emission after multiple cycles, as indicated earlier, but also because they show an increment in their lifetime after going back to vacuum, as shown in Figure 5. Additionally, in the cases of Ar, N_2, and O_2, a passivation effect is visible since the lifetime ratio becomes lower than 1. This also reveals a minor enhancement of charge transport in the crystallites since PL lifetime becomes longer. Moreover, the small lifetime fluctuations at different pressure points for all gases signals the

5. Conclusion

To summarize, we investigated the effect that atmospheric gases such as argon, molecular nitrogen, molecular oxygen, and water-enriched argon have on the PL emission of triple-cation

perovskite layers. Using the SV-analysis, we found that the perovskite crystals are mostly statically quenched by all the gases and that the effect is reversible. Additionally, dynamic and static quenching, along with passivation of boundary defects, occur simultaneously for all gases at different pressures. The strongest PLQ effects were displayed in atmospheres of O_2 and H_2O, where PL emissions were reduced by more than 20% at a low partial pressure of 1 mbar. O_2 quenches more than half of the accessible emitters at a pressure of 10 mbar, showing that its effect mostly occurs at the crystallites surface via excitation energy transfer to O_2, forming a singlet oxygen. For H_2O, we find the MHP energy levels closely align with the redox potential for water splitting, making it possible for charges to be transferred from an excited perovskite crystallite to a water molecule leading to the observed PLQ. Lastly, Ar and N_2 showed a notable PL quenching effect due to VdW complex formation. At 1000 mbar of pressure, O_2, H_2O, N_2, and Ar reduced the PL emission of pristine samples by 74%, and 63%, 49% and 34%, respectively. These findings highlight the importance of controlling and minimizing the access of contaminant gases inside of gloveboxes during preparation and characterization of perovskite samples. Furthermore, they emphasize the importance of using low photon flux illumination sources to avoid the emergence of artificial physical effects.

6. Experimental Section

Sample Preparation: The triple-cation perovskite samples were prepared as described in ref. [9]. Lead iodide and lead bromide were purchased from Tokyo Chemical Industry Company Limited, formamidinium iodide and methylammonium bromide were purchased from Dyenamo AB, and cesium iodide from Abcr GmbH. Dimethylformamide, dimethylsulfoxide, and ethyl acetate were purchased from Sigma-Aldrich. All samples were spin coated on microscope glass slides (VWR) at 4000 rpm for 35 s, with an acceleration of 5 s. Ethyl acetate was used as antisolvent after 25 s of starting the process. Annealing was done at 100 °C for 45 min. Samples were stored in vials sealed inside of a nitrogen-filled glovebox before PL characterization.

Characterization Methods: PL emission and PL lifetime were analyzed with an Edinburgh FLS980 spectrometer, equipped with a 450 W xenon arc lamp. Numerical fitting is done via an exponential tail fit analysis provided by Edinburgh instruments Ltd. The lifetime analyses are done by intensity-weighted averages of the lifetimes emerging from the double-exponential fit. The equation is of the form

$$\tau = \frac{a_1\,\tau_1^2 + a_2\,\tau_2^2}{a_1\,\tau_1 + a_2\,\tau_2} \quad (7)$$

where a_1 and a_2 are the amplitudes of the fitted lifetimes τ_1 and τ_2. These terms are part of the double-exponential decay function

$$F(t) = a_1\,e^{-t/\tau_1} + a_2\,e^{-t/\tau_2} \quad (8)$$

The resulting average lifetime τ corresponds to an approximation of a single exponential fit. We also would like to emphasize that this lifetime is not power dependent, as shown in Section 4.

Samples were excited at 510 nm and recorded at 760 nm. Lifetime measurements used a picosecond pulsed diode laser EPL-510 with a period of 10 µm. All samples were briefly exposed to air before being fixed into a cryostat where the measurement would take place. After securing a sample, Ar was flushed into the cryostat for 10 min. Then, the chamber was emptied down to 0.02 mbar and filled with Ar three times to ensure a quencher free atmosphere on the sample. The effect of each gas was later measured at different pressures, starting from as low as 0.017 mbar up to 1000 mbar. For the samples measured at

1 atm, the samples were fixed on a sealed chamber where the same gases were constantly flushed at an overpressure no larger than 5 mbar. Power intensities of the Xenon lamp and laser were measured with a Thorlabs PM100A power meter. Scanning electron microscopy images were done with a cold emission gun S4100 by Hitachi. X-ray diffraction analysis was done in air with a Bruker D8 Advance using Bragg Brentano geometry and equipped with a Cu-Kalpha anode.

Information on Gases Used: All gases were purchased from Air Liquide: "Argon Alphagaz 2 Ar" contains impurities of <0.5 ppm-mol of water and <0.1 ppm-mol of O_2, KW, CO, CO_2, and H_2; "Nitrogen Alphagaz 2 N_2" contains <0.5 ppm-mol of water and <0.1 ppm-mol of O_2, KW, CO, CO_2, and H_2; "Oxygen N48" contains <2 ppmv of water and <0.2 ppm-mol of KW, CO, and CO_2. Special versions of "Argon N50" (with 5, 2, and 0.5 ppmv of N_2, O_2, and KW, respectively) were prepared by Air Liquide upon request with 10, 50, and 100 ppm-mol of water.

Supporting Information

Supporting Information is available from the Wiley Online Library or from the author.

Acknowledgements

Conflict of Interest

The authors declare no conflict of interest.

Keywords

[1] S. D. Stranks, G. E. Eperon, G. Grancini, C. Menelaou, M. J. P. Alcocer, T. Leijtens, L. M. Herz, A. Petrozza, H. J. Snaith, *Science* **2013**, *342*, 341.

[2] D. W. Dequilettes, S. Koch, S. Burke, R. K. Paranji, A. J. Shropshire, M. E. Ziffer, D. S. Ginger, *ACS Energy Lett.* **2016**, *1*, 438.

[3] T. Leijtens, G. E. Eperon, A. J. Barker, G. Grancini, W. Zhang, J. M. Ball, A. R. S. Kandada, H. J. Snaith, A. Petrozza, *Energy Environ. Sci.* **2016**, *9*, 3472.

[4] M. A. Green, E. D. Dunlop, D. H. Levi, J. Hohl-Ebinger, M. Yoshita, A. W. Y. Ho-Baillie, *Prog. Photovoltaics Res. Appl.* **2019**, *27*, 565.

[5] Y. Tian, M. Peter, E. Unger, M. Abdellah, K. Zheng, T. Pullerits, A. Yartsev, V. Sundström, I. G. Scheblykin, *Phys. Chem. Chem. Phys.* **2015**, *17*, 24978.

[6] R. Brenes, C. Eames, V. Bulović, M. S. Islam, S. D. Stranks, *Adv. Mater.* **2018**, *30*, 1706208.

[7] N. Aristidou, I. Sanchez-Molina, T. Chotchuangchutchaval, M. Brown, L. Martinez, T. Rath, S. A. Haque, *Angew. Chem., Int. Ed.* **2015**, *54*, 8208.

[8] G. Xie, L. Xu, L. Sun, Y. Xiong, P. Wu, B. Hu, *J. Mater. Chem. A* **2019**, *7*, 5779.

[9] M. Saliba, J.-P. Correa-Baena, C. M. Wolff, M. Stolterfoht, N. Phung, S. Albrecht, D. Neher, A. Abate, *Chem. Mater.* **2018**, *30*, 4193.

[10] M. Saliba, T. Matsui, J.-Y. Seo, K. Domanski, J.-P. Correa-Baena, M. K. Nazeeruddin, S. M. Zakeeruddin, W. Tress, A. Abate, A. Hagfeldt, M. Gratzel, *Energy Environ. Sci.* **2016**, *9*, 1989.

[11] E. R. Nandayapa, E. J. W. List-Kratochvil, Unpublished.

[12] D. W. H. Rankin, *Crystallogr. Rev.* **2009**, *15*, 223.

[13] G. Grancini, V. D'Innocenzo, E. R. Dohner, N. Martino, A. R. Srimath Kandada, E. Mosconi, F. De Angelis, H. I. Karunadasa, E. T. Hoke, A. Petrozza, *Chem. Sci.* **2015**, *6*, 7305.

[14] R. L. Z. Hoye, P. Schulz, L. T. Schelhas, A. M. Holder, K. H. Stone, J. D. Perkins, D. Vigil-Fowler, S. Siol, D. O. Scanlon, A. Zakutayev, A. Walsh, I. C. Smith, B. C. Melot, R. C. Kurchin, Y. Wang, J. Shi, F. C. Marques, J. J. Berry, W. Tumas, S. Lany, V. Stevanović, M. F. Toney, T. Buonassisi, *Chem. Mater.* **2017**, *29*, 1964.

[15] H. Jin, E. Debroye, M. Keshavarz, I. G. Scheblykin, M. B. J. Roeffaers, J. Hofkens, J. A. Steele, *Mater. Horiz.* **2020**, *7*, 397.

[16] I. Levine, O. G. Vera, M. Kulbak, D.-R. Ceratti, C. Rehermann, J. A. Márquez, S. Levcenko, T. Unold, G. Hodes, I. Balberg, D. Cahen, T. Dittrich, *ACS Energy Lett.* **2019**, *4*, 1150.

[17] F. S. Zu, P. Amsalem, I. Salzmann, R. Bin Wang, M. Ralaiarisoa, S. Kowarik, S. Duhm, N. Koch, *Adv. Opt. Mater.* **2017**, *5*, 1700139.

[18] S. Pont, D. Bryant, C.-T. LIN, N. Aristidou, S. Wheeler, X. Ma, R. Godin, S. A. Haque, J. Durrant, *J. Mater. Chem. A* **2017**, *5*, 9553.

[19] D. Bryant, N. Aristidou, S. Pont, I. Sanchez-Molina, T. Chotchunang atchaval, S. Wheeler, J. R. Durrant, S. A. Haque, *Energy Environ. Sci.* **2016**, *9*, 1655.

[20] A. Senocrate, T. Acartürk, G. Y. Kim, R. Merkle, U. Starke, M. Grätzel, J. Maier, *J. Mater. Chem. A* **2018**, *6*, 10847.

[21] N. Aristidou, C. Eames, I. Sanchez-Molina, X. Bu, J. Kosco, M. Saiful Islam, S. A. Haque, *Nat. Commun.* **2017**, *8*, 15218.

[22] C.-T. Lin, F. De Rossi, J. Kim, J. Baker, J. Ngiam, B. Xu, S. Pont, N. Aristidou, S. A. Haque, T. Watson, M. A. McLachlan, J. R. Durrant, *J. Mater. Chem. A* **2019**, *7*, 3006.

[23] J. F. Galisteo-López, M. Anaya, M. E. Calvo, H. Míguez, *J. Phys. Chem. Lett.* **2015**, *6*, 2200.

[24] H.-H. Fang, S. Adjokatse, H. Wei, J. Yang, G. R. Blake, J. Huang, J. Even, M. A. Loi, *Sci. Adv.* **2016**, *2*, e1600534.

[25] S. G. Motti, M. Gandini, A. J. Barker, J. M. Ball, A. R. Srimath Kandada, A. Petrozza, *ACS Energy Lett.* **2016**, *1*, 726.

[26] M. Anaya, J. F. Galisteo-López, M. E. Calvo, J. P. Espinós, H. Míguez, *J. Phys. Chem. Lett.* **2018**, *9*, 3891.

[27] Z. Wang, Q. Lin, B. Wenger, M. G. Christoforo, Y. H. Lin, M. T. Klug, M. B. Johnston, L. M. Herz, H. J. Snaith, *Nat. Energy* **2018**, *3*, 855.

[28] C. Law, L. Miseikis, S. Dimitrov, P. Shakya-Tuladhar, X. Li, P. R. F. Barnes, J. Durrant, B. C. O'Regan, *Adv. Mater.* **2014**, *26*, 6268.

[29] M. I. Dar, G. Jacopin, S. Meloni, A. Mattoni, N. Arora, A. Boziki, S. M. Zakeeruddin, U. Rothlisberger, M. Grätzel, *Sci. Adv.* **2016**, *2*, e1601156.

[30] N. H. Nickel, F. Lang, V. V. Brus, O. Shargaieva, J. Rappich, *Adv. Electron. Mater.* **2017**, *3*, 1700158.

[31] C.-R. Ke, A. Walton, D. J. Lewis, A. A. Tedstone, P. O'Brien, A. Thomas, W. Flavell, *Chem. Commun.* **2017**, *53*, 5231.

[32] N. Z. Koocher, D. Saldana-Greco, F. Wang, S. Liu, A. M. Rappe, *J. Phys. Chem. Lett.* **2015**, *6*, 4371.

[33] E. Mosconi, J. M. Azpiroz, F. De Angelis, *Chem. Mater.* **2015**, *27*, 4885.

[34] J. Yang, Z. Yuan, X. Liu, S. Braun, Y. Li, J. Tang, F. Gao, C. Duan, M. Fahlman, Q. Bao, *ACS Appl. Mater. Interfaces* **2018**, *10*, 16225.

[35] M. Ralaiarisoa, I. Salzmann, F. S. Zu, N. Koch, *Adv. Electron. Mater.* **2018**, *4*, 1800307.

[36] F. Zu, C. M. Wolff, M. Ralaiarisoa, P. Amsalem, D. Neher, N. Koch, *ACS Appl. Mater. Interfaces* **2019**, *11*, 21578.

[37] J. S. Yun, A. Ho-Baillie, S. Huang, S. H. Woo, Y. Heo, J. Seidel, F. Huang, Y. B. Cheng, M. A. Green, *J. Phys. Chem. Lett.* **2015**, *6*, 875.

[38] G. W. P. Adhyaksa, S. Brittman, H. Āboliņš, A. Lof, X. Li, J. D. Keelor, Y. Luo, T. Duevski, R. M. A. Heeren, S. R. Ellis, D. P. Fenning, E. C. Garnett, *Adv. Mater.* **2018**, *30*, 1804792.

[39] M. Abdi-Jalebi, Z. Andaji-Garmaroudi, S. Cacovich, C. Stavrakas, B. Philippe, J. M. Richter, M. Alsari, E. P. Booker, E. M. Hutter, A. J. Pearson, S. Lilliu, T. J. Savenije, H. Rensmo, G. Divitini, C. Ducati, R. H. Friend, S. D. Stranks, *Nat. Publ. Gr.* **2018**, *555*, 497.

[40] M. Abdi-Jalebi, Z. Andaji-Garmaroudi, A. J. Pearson, G. Divitini, S. Cacovich, B. Philippe, H. Rensmo, C. Ducati, R. H. Friend, S. D. Stranks, *ACS Energy Lett.* **2018**, *3*, 2671.

[41] S. H. Turren Cruz, M. Saliba, M. T. Mayer, H. Juarez Santiesteban, X. Mathew, L. Nienhaus, W. Tress, M. P. Erodici, M.-J. Sher, M. G. Bawendi, M. Grätzel, A. Abate, A. Hagfeldt, J.-P. Correa-Baena, *Energy Environ. Sci.* **2017**, *11*, 78.

[42] B. Philippe, M. Saliba, J.-P. Correa-Baena, U. B. Cappel, S.-H. Turren-Cruz, M. Grätzel, A. Hagfeldt, H. Rensmo, *Chem. Mater.* **2017**, *29*, 3589.

[43] Y. Hu, E. M. Hutter, P. Rieder, I. Grill, J. Hanisch, M. F. Aygüler, A. G. Hufnagel, M. Handloser, T. Bein, A. Hartschuh, K. Tvingstedt, V. Dyakonov, A. Baumann, T. J. Savenije, M. L. Petrus, P. Docampo, *Adv. Energy Mater.* **2018**, *8*, 1703057.

[44] Y. Zong, Y. Zhou, Y. Zhang, Z. Li, L. Zhang, M. G. Ju, M. Chen, S. Pang, X. C. Zeng, N. P. Padture, *Chem* **2018**, 1.

[45] Y. Chen, N. Li, L. Wang, L. Li, Z. Xu, H. Jiao, P. Liu, C. Zhu, H. Zai, M. Sun, W. Zou, S. Zhang, G. Xing, X. Liu, J. Wang, D. Li, B. Huang, Q. Chen, H. Zhou, *Nat. Commun.* **2019**, *10*, 1112.

[46] J.-W. Lee, S.-H. Bae, N. De Marco, Y.-T. Hsieh, Z. Dai, Y. Yang, *Mater. Today Energy* **2018**, *7*, 149.

[47] Q. Jiang, Y. Zhao, X. Zhang, X. Yang, Y. Chen, Z. Chu, Q. Ye, X. Li, Z. Yin, J. You, *Nat. Photonics* **2019**, *13*, 460.

[48] L. Kegelmann, P. Tockhorn, C. M. Wolff, J. A. Márquez, S. Caicedo-Dávila, L. Korte, T. Unold, W. Lövenich, D. Neher, B. Rech, S. Albrecht, *ACS Appl. Mater. Interfaces* **2019**, *11*, 9172.

[49] M. R. Ayers, A. J. Hunt, *J. Non-Cryst. Solids* **1998**, *225*, 343.

[50] M. Kasha, A. U. Khan, *Ann. N. Y. Acad. Sci.* **1970**, *171*, 5.

[51] A. Köhler, H. Bässler, *Electronic Processes in Organic Semiconductors*, Wiley-VCH Verlag GmbH & Co. KGaA, Weinheim, Germany **2015**.

[52] M. Baranowski, P. Plochocka, *Adv. Energy Mater.* **2020**, *10*, 1903659.

[53] M. A. Becker, R. Vaxenburg, G. Nedelcu, P. C. Sercel, A. Shabaev, M. J. Mehl, J. G. Michopoulos, S. G. Lambrakos, N. Bernstein, J. L. Lyons, T. Stöferle, R. F. Mahrt, M. V. Kovalenko, D. J. Norris, G. Rainò, A. L. Efros, *Nature* **2018**, *553*, 189.

[54] V. D'Innocenzo, G. Grancini, M. J. P. Alcocer, A. R. S. Kandada, S. D. Stranks, M. M. Lee, G. Lanzani, H. J. Snaith, A. Petrozza, *Nat. Commun.* **2014**, *5*, 3586.

[55] B. Valeur, M. N. Berberan-Santos, *Molecular Fluorescence*, Wiley-VCH Verlag GmbH & Co. KGaA, Weinheim, Germany **2012**.

[56] X. Gong, M. Li, X.-B. Shi, H. Ma, Z.-K. Wang, L.-S. Liao, *Adv. Funct. Mater.* **2015**, *25*, 6671.

[57] J. Zhang, P. Zhou, J. Liu, J. Yu, *Phys. Chem. Chem. Phys.* **2014**, *16*, 20382.

[58] L. Ling, S. Yuan, P. Wang, H. Zhang, L. Tu, J. Wang, Y. Zhan, L. Zheng, *Adv. Funct. Mater.* **2016**, *26*, 5028.

[59] J. M. Frost, K. T. Butler, F. Brivio, C. H. Hendon, M. van Schilfga arde, A. Walsh, *Nano Lett.* **2014**, *14*, 2584.

[60] J. H. Joo, R. Merkle, J. Maier, *J. Power Sources* **2011**, *196*, 7495.

[61] C. G. Zoski, *Handbook of Electrochemistry*, Elsevier, Las Cruces, New Mexico, USA **2007**.

[62] H. Kisch, *Semiconductor Photocatalysis*, Wiley-VCH Verlag GmbH & Co. KGaA, Weinheim, Germany **2014**.

[63] *Photoelectrochemical Water Splitting* (Eds: H.-J. Lewerenz, L. Peter), Royal Society of Chemistry, Cambridge **2013**.

**ADVANCED
SCIENCE NEWS**

www.advancedsciencenews.com

**ADVANCED
OPTICAL
MATERIALS**

www.advopticalmat.de

[64] M. E. Frink, D. Magde, D. Sexton, P. C. Ford, *Inorg. Chem.* **1984**, *23*, 1238.

[65] M. C. Cuquerella, F. Boscá, M. A. Miranda, *J. Org. Chem.* **2004**, *69*, 7256.

[66] S. Simoncelli, G. Kuzmanich, M. N. Gard, M. A. Garcia-Garibay, *J. Phys. Org. Chem.* **2010**, *23*, 376.

[67] G. Albino de Souza, T. Duque Martins, F. Colmati, in *Biosens. Environ. Monit.*, IntechOpen, London **2019**.

[68] M. M. Martin, J. T. Hynes, *Femtochemistry and Femtobiology*, Elsevier, New York **2004**.

[69] J. Manz, L. Wöste, *Femtosecond Chemistry*, Wiley, New York **1994**.

[70] *Advances in Laser Chemistry* (Ed: A. H. Zewail), Springer, Berlin **1978**.

[71] A. Amirav, U. Even, J. Jortner, *Chem. Phys. Lett.* **1980**, *72*, 16.

[72] S. Sambursky, G. Wolfsohn, *Nature* **1946**, *157*, 228.

[73] V. M. Zhyrovetsky, D. I. Popovych, S. S. Savka, A. S. Serednytski, *Nanoscale Res. Lett.* **2017**, *12*, 132.

[74] S. D. Stranks, V. M. Burlakov, T. Leijtens, J. M. Ball, A. Goriely, H. J. Snaith, *Phys. Rev. Appl.* **2014**, *2*, 034007.

[75] H. Wang, L. Whittaker-Brooks, G. R. Fleming, *J. Phys. Chem. C* **2015**, *119*, 19590.

[76] T. S. Sherkar, C. Momblona, L. Gil-Escrig, J. Ávila, M. Sessolo, H. J. Bolink, L. J. A. Koster, *ACS Energy Lett.* **2017**, *2*, 1214.

[77] Z. V. Vardeny, *Ultrafast Dynamics and Laser Action of Organic Semiconductors*, CRC Press, Boca Raton, Florida **2009**.

[78] O. Stern, M. Volmer, *Z. Phys.* **1919**, *20*, 183.

[79] A. V. Popov, V. S. Gladkikh, A. I. Burshtein, *J. Phys. Chem. A* **2003**, *107*, 8177.

[80] J. R. Lakowicz, G. Weber, *Biochemistry* **1973**, *12*, 4161.

[81] S. S. Lehrer, *Biochemistry* **1971**, *10*, 3254.

[82] W. R. Ware, *J. Phys. Chem.* **1962**, *66*, 455.

[83] S. Izakura, W. Gu, R. Nishikubo, A. Saeki, *J. Phys. Chem. C* **2018**, *122*, 14425.

[84] H. C. Fry, D. V. Scaltrito, K. D. Karlin, G. J. Meyer, *J. Am. Chem. Soc.* **2003**, *125*, 11866.

[85] J. Z. Ou, W. Ge, B. Carey, T. Daeneke, A. Rotbart, W. Shan, Y. Wang, Z. Fu, A. F. Chrimes, W. Wlodarski, S. P. Russo, Y. X. Li, K. Kalantar-Zadeh, *ACS Nano* **2015**, *9*, 10313.

[86] J. K. Chen, S. M. Yang, B. H. Li, C. H. Lin, S. Lee, *Langmuir* **2018**, *34*, 1441.

[87] W. Wu, J. Sun, J. Ji, W. Wu, J. Zhao, H. Guo, *Dalton Trans.* **2011**, *40*, 11550.

[88] N. Kuramoto, *J. Soc. Dyers Colour.* **1990**, *106*, 181.

[89] B. Nacht, C. Larndorfer, S. Sax, S. M. Borisov, M. Hajnsek, F. Sinner, E. J. W. List-Kratochvil, I. Klimant, *Biosens. Bioelectron.* **2015**, *64*, 102.

[90] H. Hintz, H.-J. Egelhaaf, L. Lüer, J. Hauch, T. Peisert, T. Chassé, *Chem. Mater.* **2011**, *23*, 145.

[91] J. R. Lakowicz, *Principles of Fluorescence Spectroscopy*, Springer US, Boston, MA **2006**.

[92] E. R. Carraway, J. N. Demas, B. A. DeGraff, *Anal. Chem.* **1991**, *63*, 332.

[93] L. Sacksteder, J. N. Demas, B. A. DeGraff, *Anal. Chem.* **1993**, *65*, 3480.

[94] J. N. Demas, B. A. DeGraff, W. Xu, *Anal. Chem.* **1995**, *67*, 1377.

[95] C. Wang, W. Lin, *J. Am. Chem. Soc.* **2011**, *133*, 4232.